Journal of Materials Chemistry C

ROYAL SOCIETY OF CHEMISTRY

PAPER

View Article Online
View Journal

Cite this: DOI: 10.1039/d5tc00226e

Hybrid $CsPbBr_3$ superlattice/Ag microcavity enabling strong exciton–photon coupling for low-threshold continuous-wave pumped polariton lasing†

Zhenxu Lin,[ab] Rui Huang,*[a] Shulei Li,*[c] Mingcheng Panmai,[d] Yi Zhang,[a] Haixia Wu,[a] Jie Song,[a] Zewen Lin,[a] Hongliang Li[a] and Sheng Lan*[b]

Achieving strong exciton–photon coupling in perovskite microcavities opens new possibilities for continuous-wave (CW) perovskite lasers with ultralow thresholds. A $CsPbBr_3$ superlattice (SL), assembled from quantum dots (QDs) with a narrow size distribution, offers both large oscillator strengths and extended exciton dephasing times, rendering it a highly promising platform for enhanced light–matter interactions. Nevertheless, realizing robust exciton–photon coupling in a $CsPbBr_3$ SL-based microcavity for low-threshold lasing remains elusive. Here, we demonstrate a hybrid microcavity integrating a $CsPbBr_3$ SL with a thin Ag film to boost exciton–photon coupling and achieve CW-pumped polariton lasing. Using an acetone-assisted self-assembly approach, we obtain high-quality $CsPbBr_3$ SLs characterized by narrow emission linewidths, large exciton binding energies, diminished exciton–phonon coupling, and highly stable amplified spontaneous emission. Optical scattering and photoluminescence measurements indicate significant coupling between the SL excitons and resonant photon modes in the $CsPbBr_3$/Ag microcavity. We attribute this enhanced light–matter interaction to comparable linewidths of the exciton resonance and photon mode, facilitated by the Ag film. A coupled oscillator model fit yields a Rabi splitting of approximately 225 meV in a large microcavity. Notably, we achieve CW-pumped polariton lasing near the lower polariton branch bottleneck at a low threshold of about 220 W cm^{-2}. Our findings elucidate the fundamental mechanism underlying strong exciton–photon coupling in $CsPbX_3$ SL systems and offer a viable strategy for designing CW-pumped polariton lasers with improved performance.

Received 18th January 2025,
Accepted 21st April 2025

DOI: 10.1039/d5tc00226e

rsc.li/materials-c

Introduction

Strong exciton–photon coupling in a cesium lead halide ($CsPbX_3$, X = Cl, Br, I) perovskite microcavity leads to the formation of microcavity polaritons with part-matter and part-light features.[1–3] Being as bosons with low effective mass and strong coherence, microcavity polaritons emerge as a promising candidate for exploring room temperature collective phenomena, such as Bose–Einstein condensation and polariton lasing *etc.* This unique feature makes it possible to realize a polariton laser with a threshold many orders of magnitude lower than that of traditional photonic lasers, which is limited by the population inversion condition.[4–8] The dramatic reduction in lasing threshold is beneficial to the realization of continuous wave (CW) pumped $CsPbX_3$ lasers. So far, CW-pumped polariton lasing has been achieved in planar micro-/nano cavities based on single crystalline $CsPbX_3$.[9–11] Very recently, Song *et al.* demonstrated a CW-pumped $CsPbBr_3$ laser by using a microplatelet with an area smaller than 1 μm^2. The low threshold of $\sim$0.84 kW cm^{-2} was achieved by exploiting the strong exciton–photon coupling.[11] From the viewpoint of practical application, however, a further improvement is still necessary in order to realize a CW-pumped polariton laser with an ultralow threshold at room temperature.

In recent years, $CsPbX_3$ quantum dots (QDs) have attracted great interest because of their high photoluminescence quantum yields (PLQYs) and narrow emission line widths.[12–14] As compared with bulk materials, low-dimensional $CsPbX_3$, such as QDs, possess larger exciton binding energy (E_b) resulting from the weaker dielectric screening and higher confinement effect,

[a] School of Physics and Electronic Engineering, Hanshan Normal University, Chaozhou 521041, China. E-mail: rhuang@hstc.edu.cn
[b] Guangdong Provincial Key Laboratory of Nanophotonic Functional Materials and Devices, School of Information and Optoelectronic Science and Engineering, South China Normal University, Guangzhou 510006, China. E-mail: slan@scnu.edu.cn
[c] School of Optoelectronic Engineering, Guangdong Polytechnic Normal University, Guangzhou 510665, China. E-mail: shuleili@gpnu.edu.cn
[d] Division of Physics and Applied Physics, School of Physical and Mathematical Sciences, Nanyang Technological University, Singapore, 637371, Singapore

† Electronic supplementary information (ESI) available. See DOI: https://doi.org/10.1039/d5tc00226e

facilitating the formation of exciton–photon polaritons at room temperature.[15–17] Apart from the larger E_b, the reduced dielectric screening in low-dimensional $CsPbX_3$ leads to an enhancement in exciton oscillator strength. Since the exciton–photon coupling strength g is governed by the relation $g \propto \sqrt{N \times f/V}$, where N is the number of excitons, f is the exciton oscillator strength and V is the photonic mode volume, it is believed that a microcavity composed of $CsPbX_3$ QDs can be employed to enhance the exciton–photon interaction, leading to a large Rabi splitting energy (Ω).[18] Remarkably, formation exciton–photon polaritons with a Rabi splitting energy of $\Omega \sim 127.5$ meV has been demonstrated in a microcavity composed of $CsPbX_3$ QD monolayers and a planar optical microcavity created by the combination of metallic mirrors and distributed Bragg reflectors.[19] In this case, the coupling strength can be modified by the relative position between the excitonic and photonic modes. It indicates that the combination of an optical microcavity and $CsPbX_3$ QDs microcavity has become an ideal platform for realizing strong exciton–photon coupling. However, it is noticed that a dense film composed of $CsPbX_3$ QDs with non-uniform size distribution and defects, which is reflected in the inhomogeneous broadening of the PL spectrum, may result in enhanced exciton–phonon coupling and fast exciton dephasing, preventing the strong coupling between excitons and photons.

A $CsPbX_3$ superlattice (SL) formed by the self-assembly of $CsPbX_3$ QDs seems to be a promising candidate to overcome this shortage because it possesses long-range order and narrow size distribution of QDs.[20–25] The overlapping of electronic wave functions of QDs in the $CsPbX_3$ SL results in the delocalization of excitons, increasing exciton oscillator strength as compared with isolated QDs. Moreover, the strong electronic coupling between QDs in the $CsPbX_3$ SL leads to a low dephasing rate, which is manifested in the excitonic cooperative emission from the $CsPbX_3$ SL. This phenomenon, which is referred to as superfluorescence, has been demonstrated in $CsPbBr_3$ SLs.[26] Apart from the high-density exciton states and low dephasing rate, a $CsPbBr_3$ SLs with regular geometric shape usually supports Mie resonances, whispering gallery modes (WGMs) and Fabry–Perot (F–P) resonances, behaving as a high-quality optical microcavity with low intrinsic loss. As a result, the interaction between light and matter can be significantly enhanced, leading to enhanced superfluorescence.[27] However, less attention has been paid to the strong coupling between excitons and photons in microcavities based on $CsPbBr_3$ SLs, which can be exploited to realize CW-pumped polariton lasers.

Basically, the Rabi splitting energy Ω originating from the strong exciton–photon coupling is defined as follows:

$$\Omega = 2\sqrt{g^2 - \frac{1}{4}(\gamma_{pl} - \gamma_{ex})^2}, \quad (1)$$

where g is the coupling strength, γ_{pl} and γ_{ex} represent the dissipation rates of the optical mode and exciton transition, respectively.[28] Apparently, a direct method for obtaining a large Rabi splitting energy in a $CsPbBr_3$ SL is to increase the coupling strength, which can be achieved by increasing exciton oscillator strength, or by reducing the photonic mode volume. Alternatively, making the dissipation rate of the optical mode comparable to that of the exciton transition is also a promising way to realizing strong exciton–photon coupling in the microcavity. Basically, the optical modes supported by an all-dielectric microcavity can be modified by changing its geometrical parameters. In comparison, a metallic film can be used as a reflector to enhance the photon confinement in a dielectric microcavity.[29] Thus, a hybrid microcavity formed by a dielectric microparticle and a metal film can be employed to enhance the electric field and reduce the radiative loss, boosting exciton–photon coupling.

In this work, we successfully synthesized high-quality $CsPbBr_3$ SLs by using the self-assembly of QDs assisted by acetone. We observed stable exciton emission and weak exciton–phonon coupling in the $CsPbBr_3$ SLs by using power- and temperature-dependent PL spectra. We constructed hybrid microcavities by placing $CsPbBr_3$ SLs with different sizes on a thin Ag film and identified optical modes with high quality factors originating from the coupling of high-order Mie resonances and WGMs supported by $CsPbBr_3$ cuboids. We demonstrated the strong exciton–photon coupling with a Rabi splitting as large as $\sim$225 meV in $CsPbBr_3$/Ag hybrid microcavities and the realization of CW-pumped polariton lasers with a low threshold of $\sim$220 W cm^{-2}.

Results and discussion

The $CsPbBr_3$ SLs used in this study were prepared by the self-assembly of monodispersed QDs in hexane solution assisted by polar solvent (here acetone) (see Fig. S1(a), ESI†). The narrow size distribution of QDs and the surface ligands on QDs play a crucial role in the formation of $CsPbBr_3$ SLs. Fig. 1(a) shows the high-resolution transmission electron microscope (HR-TEM) image of pristine monodispersed $CsPbBr_3$ QDs with an average size of $\sim$10 nm, which were synthesized by using typical high temperature hot injection following the procedure reported in literature.[12] As shown in the HR-TEM image, clear lattice fringes with an interplane spacing of $\sim$0.58 nm, which is assigned to the (110) plane in the orthorhombic crystal of $CsPbBr_3$, indicate the good crystallinity of the QDs.[30] Basically, the self-assembly of QDs is driven by the intermolecular forces between aliphatic ligands.[31] Here, the ligand molecules decorated on the surfaces of QDs, which are extremely sensitive to polar solvent, are employed to fabricate $CsPbBr_3$ SLs. The fabricated $CsPbBr_3$ SLs appear as cuboids with micrometer edges, as shown in Fig. 1(b) (see also Fig. S1(c)–(e), ESI†). The elemental mapping of a typical $CsPbBr_3$ SL based on energy dispersive spectrocopy (EDS) is presented in Fig. 1(c). It indicates uniform spatial distributions for each element. The atomic ratio of Cs : Pb : Br is very close to the stoichiometry of 1 : 1 : 3 (the small deviation of the atomic ratio from the stoichiometry is caused by instrumental error). The X-ray diffraction (XRD) pattern of a $CsPbBr_3$ SL, which is shown in Fig. 1(d), exhibits two double peaks located at $\sim$15.3° and $\sim$30.6°, which are assigned to the diffractions from the (110)

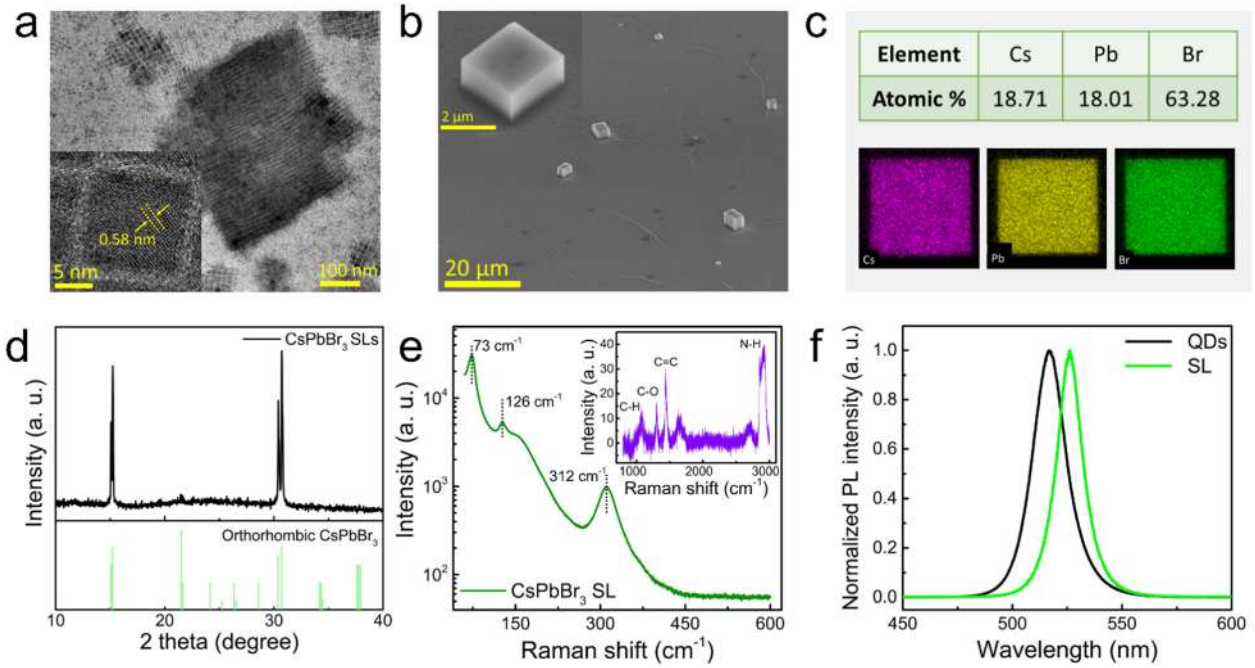

Fig. 1 (a) TEM image of monodispersed $CsPbBr_3$ QDs. The high-resolution image is shown in the inset. (b) SEM image of $CsPbBr_3$ SLs placed on an Ag film. (c) Composition analysis and EDS elemental mapping of a $CsPbBr_3$ SL. (d) XRD pattern of a $CsPbBr_3$ SL and reference peak of $CsPbBr_3$. (e) Raman spectrum of a $CsPbBr_3$ SL. (f) PL spectra of $CsPbBr_3$ QDs and a $CsPbBr_3$ SL.

and (220) faces of the orthorhombic $CsPbBr_3$ (ICSD 97851), respectively.[32] This feature, which is consistent with monodispersed QDs, confirms the existence of pure orthorhombic phase of $CsPbBr_3$ in the $CsPbBr_3$ SL. In order to characterize the local atomic environment and bonding configuration a $CsPbBr_3$ SL, we also examined the Raman spectrum of a SL, as shown in the Fig. 1(e). The three Raman modes with small wave numbers revealed in the Raman spectrum (a strong mode at 73 cm^{-1} and two weak modes at 126 and 312 cm^{-1}) are assigned to the vibrational modes of the $CsPbBr_3$ sublattice.[33] In addition, the four intense bands with large wave numbers, which are located at 1085, 1305, 1440, and 2915 cm^{-1}, are assigned to the bending vibrations of C–H, C–O, C═C, and N–H bonds, respectively.[34–36] This result implies that oleic acid/oleylamine ligands are remained on the surfaces of QDs after the self-assembly. This unique feature renders $CsPbBr_3$ SLs excellent environmental and structural stability. As compared with the PL spectrum of QDs, the PL spectrum of the SL exhibited a red shift of the PL peak from 513 to 526 nm, which is attributed to the electronic coupling of the wavefunctions in neighboring QDs of the SL.[37] In addition, a reduction in the full width at half maximum (FWHM) (from 18 to 13 nm) was observed in the SL because of the narrow size distribution of QDs. Moreover, remarkable two-photon-induced photoluminescece (TPL) was observed for the SL excited by femtosecond laser pulses and the polarization dependence of the TPL is similar to that observed in single-crystal $CsPbBr_3$ resulting from anisotropic crystal structure (Fig. S2, ESI†). All these results indicate clearly the good crystallinity of the fabricated $CsPbBr_3$ SLs. More importantly, the PL from the $CsPbBr_3$ SLs remains stable for more than 60 min at room temperature under the excitation of a 325-nm CW laser light with a power density of 140 W cm^{-2} (Fig. S3, ESI†).

It is well known that the PL from $CsPbBr_3$ QDs at room temperature originates from the radiative recombination of excitons with a high rate because the exciton binding energy in $CsPbBr_3$ QDs (40–200 meV) is larger than the thermal energy ($\sim$26 meV).[38–40] In order to understand the recombination dynamics of $CsPbBr_3$ SLs, we measured the PL spectra of a SL at different excitation power densities, as shown in Fig. 2(a). Physically, the dominant recombination process in a semiconductor with direct bandgap is generally revealed in the relationship between the integrated PL intensity (I_{PL}) and the excitation power density (I_{ex}), which is expressed as follows:[41]

$$I_{PL} \sim I_{ex}^{k}. \quad (2)$$

Here, k is a parameter associated with the dominant recombination process. In general, $k < 1$, $1 < k < 2$, and $k > 2$ represent a free-to-bound recombination or donor–acceptor pair recombination, an excitonic recombination, and a free-carrier recombination, respectively. We examine the relationship between I_{PL} and I_{ex} for a typical SL plotted in a logarithmic coordinate, as shown in the inset of Fig. 2(a). In this case, the value of k extracted from the dependence of I_{PL} on I_{ex} slope is $\sim$1.29, indicating that excitonic recombination is the dominant recombination process in the SL. This value is larger than that observed in QDs ($k \sim 0.99$, see Fig. S4, ESI†), implying an increased radiative excitonic recombination rate in the SLs. This conclusion is also supported by the longer PL lifetime

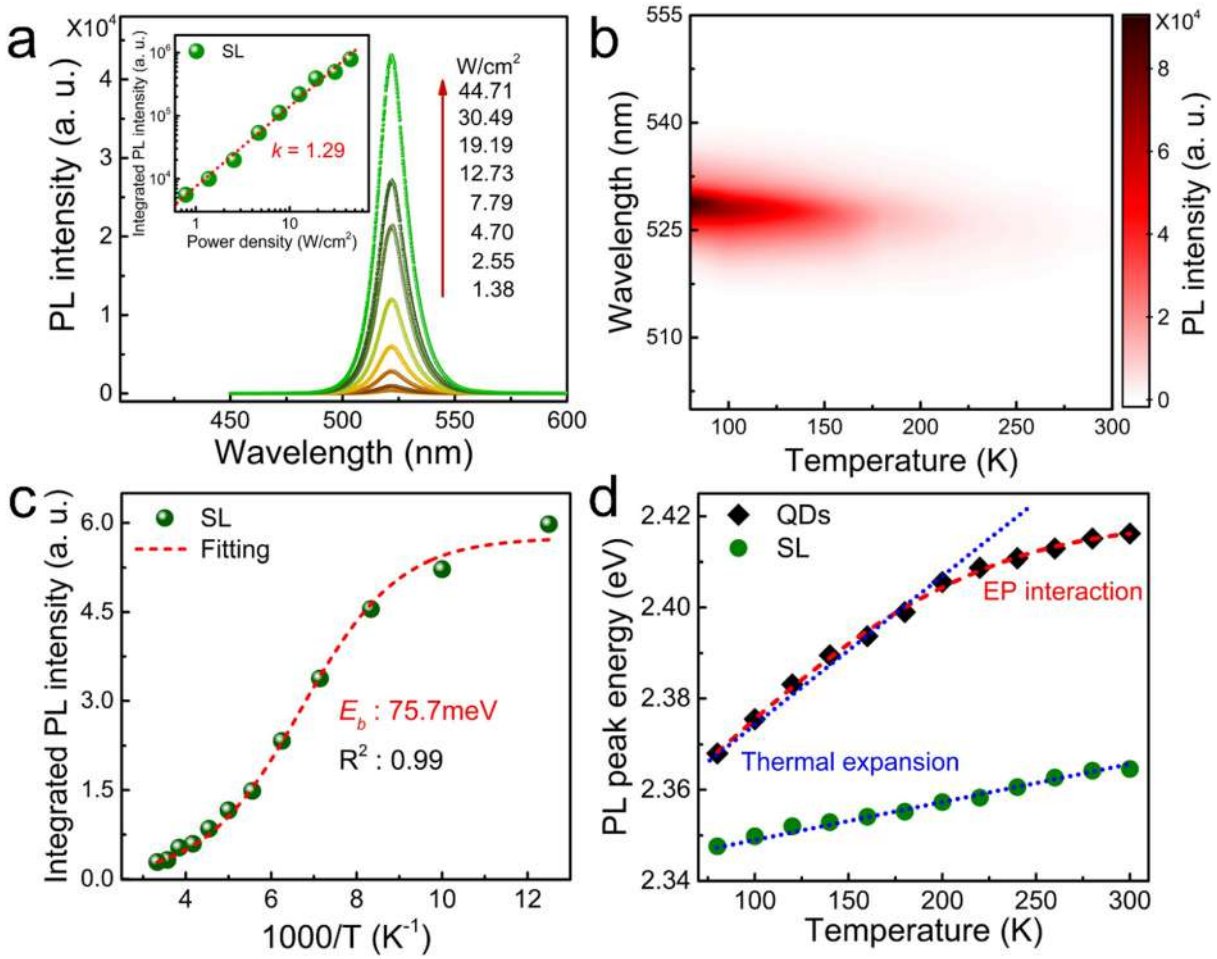

Fig. 2 (a) PL spectra of a $CsPbBr_3$ SL measured at different power densities. The inset shows the dependence of the integrated PL intensity of the $CsPbBr_3$ SL on the power density plotted in a logarithmic coordinate. (b) PL spectra of a $CsPbBr_3$ SL measured at different temperatures ranging from 80 to 300 K. (c) Dependence of the integrated PL intensity of the $CsPbBr_3$ SL on the inverse of the temperature. (d) Evolution of the PL peak with increasing temperature measured for the $CsPbBr_3$ QDs and $CsPbBr_3$ SL.

observed in the SL (Fig. S5, ESI†). We also compared the temperature-dependent PL spectra of $CsPbBr_3$ QDs and SLs, as shown in Fig. 2(b) and Fig. S6 (ESI†). Basically, the temperature-dependent PL intensity $I_{PL}(T)$ of a $CsPbBr_3$ SL can be fitted by the Arrhenius equation expressed as follows:[42]

$$I_{PL}(T) = \frac{I_{PL}(T_0)}{1 + \beta \exp(-E_b/k_B T)}. \quad (3)$$

Here, $I_{PL}(T_0)$ is the PL intensity at 80 K, β is a constant, k_B is the Boltzmann constant, and E_b is exciton binding energy, respectively. The exciton binding energy in the SL derived from the fitting of the experimental data by using with the Arrhenius equation is found to be $E_b \sim 76$ meV. This value is larger than that observed in bulk $CsPbBr_3$ microplatelets (Fig. S7, ESI†), implying a robust excitonic transition at room temperature. The large E_b is beneficial for the realization of population inversion and amplified stimulated emission (ASE) with a low threshold. As a result, we observed two-photon-pumped ASE ($\lambda = \sim 531$ nm) with a low threshold ($P_{th} \sim 0.9$ mJ cm^{-2}) in a SL at room temperature under the excitation of 800-nm femtosecond laser pulses (1 kHz, 130 fs), as shown in Fig. S8(a) and (b) (ESI†). More interestingly, the intensity of ASE remains stable for more than 60 min under a pumping power density of $1.45P_{th}$ (Fig. S8(c), ESI†), implying a potential application for lasing application. In Fig. 2(d), we present the evolution of the PL peak with increasing temperature observed for $CsPbBr_3$ QDs and SLs. Basically, the temperature-dependent PL peak (or band-gap energy) is related to the thermal expansion (TE) and exciton–phonon (EP) interaction and it can be described by the following equation:[43,44]

$$E_g(T) = E_0 + A_{TE}T + A_{EP}\left(\frac{2}{\exp(\hbar\omega/k_b T) - 1} + 1\right), \quad (4)$$

where A_{TE} and A_{EP} represent the weight of TE and EP interaction, respectively. Essentially, the enhanced EP interaction with increasing temperature will reduce the blueshift of the PL peak with increasing temperature induced by TE. As a result, a sub-linear relationship between the PL peak energy and the temperature is observed for the $CsPbBr_3$ QDs at high temperatures ($T > 200$ K). In sharp contrast, the $CsPbBr_3$ SL exhibits a linear blueshift of the

PL peak energy with increasing temperature, indicating clearly a dramatically reduced EP coupling as compared with the $CsPbBr_3$ QDs. This is considered to result from excitonic delocalization due to the electronic coupling of neighboring QDs in the SL.[24] This feature is responsible for the increased radiative recombination rate and enhanced PLQY observed for the $CsPbBr_3$ SLs. Thus, the $CsPbBr_3$ SLs fabricated in this way exhibit great potential in the fabrication of pervoskite lasers with low thresholds operating at room temperature.

Basically, a $CsPbBr_3$ SL with a regular geometric shape and a moderate refractive index (n = 2.3) can serve as an optical microcavity that provides necessary optical feedback for light amplification. Previous studies have demonstrated that cavity-enhanced superfluorescence can be achieved in a $CsPbBr_3$ SL assembled by from $CsPbBr_3$ QDs.[27] Thus, it would be interesting to find out whether the optical modes supported by a $CsPbBr_3$ SL microcavity can be exploited to the enhance light–matter interaction. In Fig. S9 (ESI†), we show the optical resonances observed in the forward scattering spectra of SLs with different sizes placed on a SiO_2 substrate by using polarized white light and analyzer with cross polarization. It was previously reported that the coupling between a narrow exciton resonance and a broader cavity mode lead to the formation of asymmetric Fano resonance, making it difficult to reveal the larger Rabi splitting from exciton–photon coupling.[45] Based on previous studies, the light–matter interaction can be greatly enhanced by constructing a hybrid cavity composed of a $CsPbBr_3$ particle and a thin metal film.[46–48] In particular, a significantly larger electric field enhancement factor within all-dielectric microcavities was observed for the Ag/SiO_2 substrate, attributed to the lower optical loss of Ag.[29] In this work, we created hybrid microcavities by synthesizing $CsPbBr_3$ SLs directly on a Ag/SiO_2 substrate with the conventional spin coating method. In Fig. 3(a), we show the forward scattering spectra of $CsPbBr_3$ SLs with different side length (L) placed on a Ag/SiO_2 substrate. In each case, one can identify a scattering dip in the scattering spectrum at the exciton resonance, which is resulted from the coherent coupling between the exciton resonance and the high-order Mie resonances supported by the hybrid micro-cavity. As a result, the radiative recombination of excitons can be enhanced by the Purcell effect, leading to the enhancement in the PL intensity. The corresponding electric field distribution simulation in the XZ plane calculated for such a hybrid microcavity is shown in Fig. S10 (ESI†). Here, the L and thickness of the $CsPbBr_3$ SL are assumed to be 2 μm and 0.5 μm, respectively. It is shown that the electric field distribution appears inside the $CsPbBr_3$ SL as a standing wave in both the x and z directions. In our case, the optical modes supported

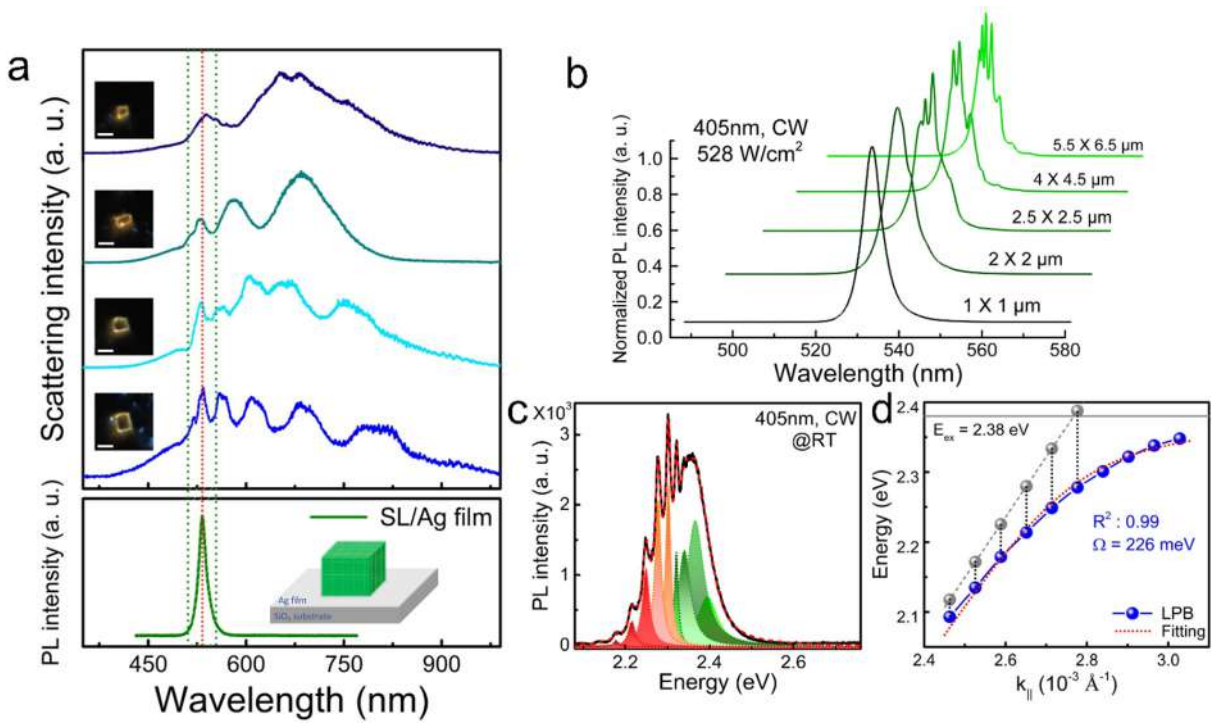

Fig. 3 (a) Forward scattering spectra measured for $CsPbBr_3$ SLs with different sizes placed on a Ag/SiO_2 substrate by using polarized white light and analyzer with cross polarization (upper panel). The corresponding optical mages of the $CsPbBr_3$ SLs recorded by using a charge coupled device (CCD) are shown in the insets. The length of the scale bar is 5 μm. Also shown is the PL spectrum of a $CsPbBr_3$ SL excited by using 405-nm CW laser light at room temperature (lower panel). The detailed configuration of the hybrid microcavity composed of a $CsPbBr_3$ SL and a Ag/SiO_2 substrate is shown in the inset. (b) PL spectra of $CsPbBr_3$ SLs with different sizes (L ranging from 1 to 6 μm) excited by using 405-nm CW laser with a power density of 528 W cm^{-2} at 80 K. (c) The PL spectrum of the $CsPbBr_3$ SL with L = 5 μm by using 405-nm CW laser light with a power density of 134 W cm^{-2} at room temperature. (d) Relationship between the energies (solid circles) of the optical modes and the wavevectors observed for the $CsPbBr_3$ SL with L = 5 μm. Also shown is the fitting of the dispersion relation by using the exciton–photon polaritons model (red dotted line).

by the hybrid microcavity may originate from the coherent interaction between the high-order Mie resonances and the WGMs or F–P resonances. It is found that the optical resonances become denser and sharper with increasing L of the SL because of the reduced optical loss, indicating that the reduced photonic mode volume for such hybrid micro-cavities. In general, the narrower linewidths or higher quality factors of the optical resonances are favorable for promoting strong coupling between the excitons and photons, creating exciton–photon polaritons. Therefore, it is expected that such hybrid microcavities are promising candidates for realizing CW-pumped pervoskite lasers with low thresholds.

In Fig. 3(b), we present the normalized PL spectra of the $CsPbBr_3$ SLs with L ranging from 1 to 6 μm placed on an Ag/SiO_2 substrate under the excitation of 405-nm CW laser light with a power density of 528 W cm^{-2}. For the $CsPbBr_3$ SLs with $L < 2$ μm, one can see only a narrow PL band without any resonant modes. In this case, the radiation loss of the microcavity is relatively large and the coupling between the excitons and photons is weak. As revealed in the scattering spectra of the SLs with small sizes (see Fig. 3(a)), the optical resonance is much broader than the linewidth of the exciton resonance. It is noticed that the multiple optical modes with narrow linewidths emerge in the scattering spectra with increasing size, indicating the enhanced exciton–photon coupling. In Fig. 3(c), we present the PL spectrum of a SL with L = 5 μm under the excitation of 405-nm CW laser light at room temperature. It is noticed that the emission peaks at the low-energy side of the PL spectrum can be well fitted by multiple Lorentz lineshapes. In addition, the free spectral range (FSR) decreases gradually when the photon energy approaches the exciton resonance (E_x), the. This feature is in good agreement with the exciton–photon polariton model, as demonstrated in previous reports.[49] In each case, the dispersion of the polaritons in the in the lower polariton branch (LPB) can be analyzed by using the Hamiltonian for the exciton–photon coupling (see Fig. S11, ESI†).[50] In Fig. 3(d), we show the fitting of the dispersion relation characterized by the dependence of the polariton energy (E) *versus* the in-plane wavevector ($k_{\parallel}$). The Rabi splitting energy extracted from the fitting of the dispersion relation is estimated to be $\Omega \sim 225$ meV, which is larger than that reported in $CsPbBr_3$ microplatelets.[11] It implies the existence of strong exciton–photon coupling in such hybrid cavities. Moreover, the PL spectra modulated by cavities and the fitting results of Rabi splitting energies for the SLs with L ranging from 3 to 5.5 μm are shown in Fig. S12 and S13 (ESI†), respectively. As L is increased from 3 to 5.5 μm, the Rabi splitting energy is increased gradually from 192 to 237 meV. This indicates that the improvement of the quality factors of the optical resonances supported by a $CsPbBr_3$ SL with increasing L facilitates the coupling with the exciton resonance. For a hybrid microcavity, the exciton–photon coupling strength depends on the exciton oscillator strength, the photonic mode volume, and

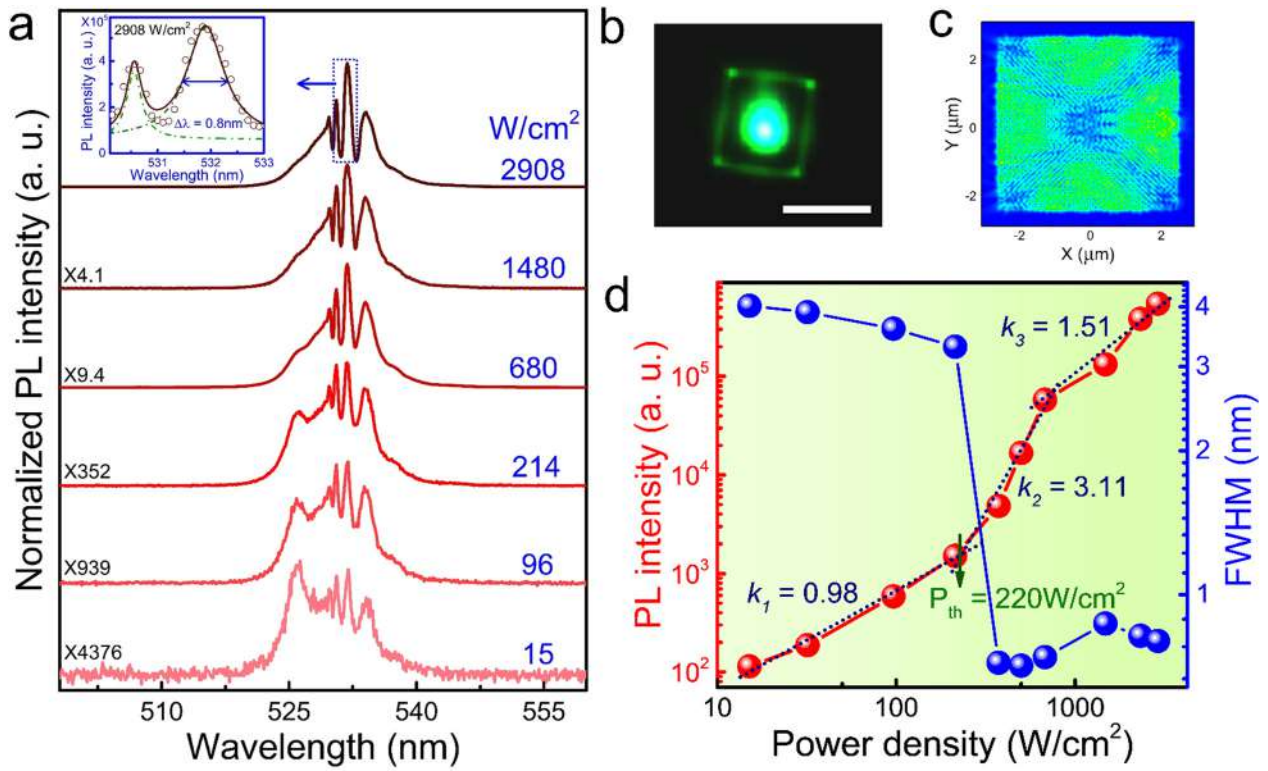

Fig. 4 (a) Normalized PL spectra measured at different excitation power densities for the $CsPbBr_3$ SL with L = 4.5 μm. The inset shows the magnified Lorentz fitted spectrum of polariton modes measured at an excitation power density of 2908 W cm^{-2}. (b) The optical image of the $CsPbBr_3$ SL. The length of the scale bar is 5 μm. (c) Electric field distributions in the *xy* plane calculated at 530 nm for a $CsPbBr_3$ SL placed on a Ag/SiO_2 substrate. (d) The PL intensity and FWHM of dominant emission peak as a function of excitation power density.

the linewidth match between the optical mode and the exciton resonance. As compared with bulk $CsPbBr_3$, the oscillator strength of the excitons in a $CsPbBr_3$ SL is increased by the coherent coupling of excitons induced by the reduced interdot distance and EP interaction. As a result, the exciton–photon coupling is enhanced, resulting in a larger Rabi splitting energy. On the other hand, it is well known that the effective mode volume is inversely proportional to the quality factor of the photonic mode. The confinement of light in the microcavity is governed by the group refractive index n_g (Fig. S14, ESI†). When L is increased from 2.5 to 4.25 μm, the group refractive index n_g is increased from 15 to 26.4. It implies that the light confinement becomes more efficient in large SLs. Therefore, a stronger exciton–photon coupling can be achieved in $CsPbBr_3$ SLs with large sizes ($L > 2$ μm), which is benefit for the realization of polariton lasing under the excitation of CW laser light.

In Fig. 4(a), we show the PL spectra of a large $CsPbBr_3$ SL with L = 4.5 μm (the thickness is 0.6 μm, see Fig. S15, ESI†) obtained at different excitation power densities. The $CsPbBr_3$ SL was excited by using 405-nm CW laser light at 80 K. At a power density of 15 W cm^{-2}, the PL spectrum is dominated by a broad SE peak centered at 526.5 nm with a FWHM of ~4 nm. Meanwhile, several narrow oscillation peaks with nonidentical spacing, which are attributed to the optical modes selectively amplified by the optical gain in a square $CsPbBr_3$ SL, appear on the low energy side of the SE peak. From the optical image of the SL (see Fig. 4(b)), one can see bright green light emission from four corners of the SL, suggesting that the dominant optical mode is the WGMs supported by the $CsPbBr_3$ SL.[51] This is consistent with the electric field distribution calculated for the hybrid microcavity, which shows notable leakage at the four corners (see Fig. 4(c)). In Fig. 4(d), one can see a rapid increase in the PL intensities of the oscillation peaks when the power density is further is increased. As the power density reaches 220 W cm^{-2}, the dependence of the PL intensity on the excitation power density exhibits a transition from a sublinear to a superlinear relationship. Moreover, the linewidth of dominant emission peak is dramatically reduced to ~0.8 nm, indicating clearly the appearance of multi-mode lasing (see the inset of Fig. 4(a)). In addition, it was found that the decay time drops rapidly to the order of picoseconds (~380 ps) at a higher excitation fluence of 10 mJ cm^{-2} (see Fig. S16, ESI†), further confirming the lasing behavior. Thus, the lasing threshold is estimated to be P_{th} (~220 W cm^{-2}). To the best of our knowledge, the lasing threshold observed in this work is smaller than those reported in bulk $CsPbBr_3$ polariton laser,[10,11] indicating the important role of strong exciton–photon coupling achieved by using a hybrid microcavity composed of a $CsPbBr_3$ SL and a Ag thin film. Furthermore, we have also verified that the lasing behavior observed in the $CsPbBr_3$ SLs is reproducible (see Fig. S17, ESI†), indicating the stability of $CsPbBr_3$ SLs under laser illumination. More interestingly, it was found that the PL intensity from such a hybrid microcavity remains stable under continuous irradiation of 405-nm CW laser with a power density of 1480 W cm^{-2} for at least 30 min (see Fig. 5). All these phenomena indicate that

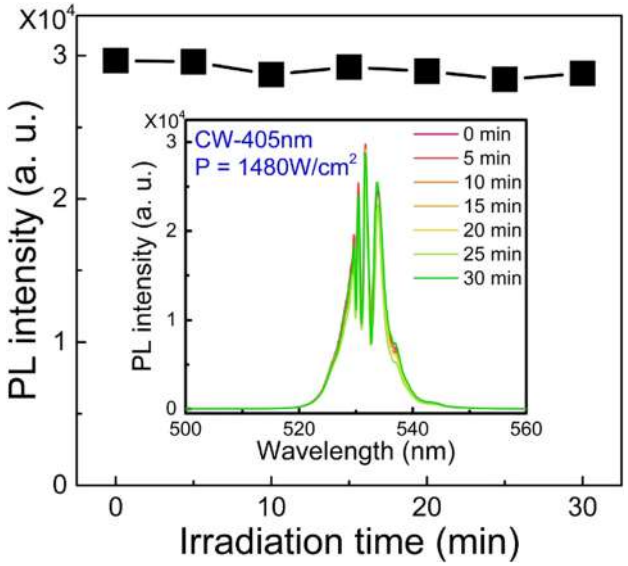

Fig. 5 PL intensity of from the $CsPbBr_3$ SL during subsequent continuous 405-nm CW laser illumination with a power density of 1480 W cm^{-2}. The inset shows the PL spectra measured for the $CsPbBr_3$ SL at different times.

such $CsPbBr_3$/Ag hybrid microcavities exhibit potential applications in realizing polariton lasers with low threshold and high stability. For comparison, we also examined the lasing behavior of a $CsPbBr_3$ SL with a similar L but with a larger thickness of ~1.1 μm (see Fig. S18, ESI†). As shown in Fig. S18(b) (ESI†), the lasing modes in the $CsPbBr_3$ SL exhibit a highly degree of polarization (DOP = 0.66), which is close to that reported in single-crystal $CsPbBr_3$ laser.[11] It was found that the lasing threshold P_{th} is increased to ~300 W cm^{-2} (see Fig. S18(c), ESI†). As shown in the optical image of the thicker $CsPbBr_3$ SL (see the inset of Fig. S18(d), ESI†), light is emitted from the four corners and the centers of four edges of the $CsPbBr_3$ SL. In the thicker $CsPbBr_3$ SL, one need to consider the F–P cavity formed by the up and bottom facets. The interplay of the WGMs and the F–P modes may degrade the light confinement in the $CsPbBr_3$ SL, leading to a higher lasing threshold.[52]

Conclusions

In summary, we have successfully synthesized $CsPbBr_3$ SLs with outstanding optical properties by using acetone-assisted self-assembly. It was found that such SLs possess narrow emission linewidths, stable exciton emission and weaker EP coupling, which were identified by excitation-power and temperature-dependent PL spectra. This unique feature makes it possible to realize strong exciton–photon coupling in SLs. We proposed the use of a hybrid microcavity composed of a SL and an Ag thin film to greatly enhanced exciton–photon coupling, resulting in a Rabi splitting as large as ~225 meV. We demonstrated polariton lasing in hybrid microcavities with a low threshold of ~220 W cm^{-2} under the excitation of CW laser light. Our findings are helpful for understanding the strong

exciton–photon coupling in $CsPbX_3$ SLs and useful for designing polariton lasers with low thresholds.

Author contributions

R. Huang and S. Lan revised paper; Z. Lin and S. Li engineered the experiments and wrote the first draft of the manuscript; H. Wu, J. Song, Z. Lin, Y. Zhang and H. Li prepared the samples and performed the photoluminescence measurements. M. Panmai and S. Li conducted numerical simulation. All authors contributed to the analysis of data and general discussion.

Data availability

The authors declare that all data supporting the results reported in this study are available within the paper and the ESI.† Additional data used for the study are available from the corresponding authors upon reasonable request.

Conflicts of interest

There are no conflicts to declare.

Acknowledgements

The authors acknowledge the financial support from the National Natural Science Foundation of China (Grant No. 11874020, 12174123, 12374347 and 12104117), Guangdong Basic and Applied Basic Research Foundation (Grant No. 2022A1515010747), Start-Up Funding of Guangdong Polytechnic Normal University (2022SDKYA007), Project of Guangdong Province Key Discipline Scientific Research Level Improvement (2021ZDJS039, 2024ZDZX1026) and Program of Hanshan Normal University (XTP202402).

Notes and references

1 X. Wang, M. Shoaib, X. Wang, X. Zhang, M. He, Z. Luo, W. Zheng, H. Li, T. Yang, X. Zhu, L. Ma and A. Pan, *ACS Nano*, 2018, **12**, 6170–6178.
2 W. Du, S. Zhang, J. Shi, J. Chen, Z. Wu, Y. Mi, Z. Liu, Y. Li, X. Sui, R. Wang, X. Qiu, T. Wu, Y. Xiao, Q. Zhang and X. Liu, *ACS Photonics*, 2018, **5**, 2051–2059.
3 R. Su, A. Fieramosca, Q. Zhang, H. S. Nguyen, E. Deleporte, Z. Chen, D. Sanvitto, T. C. H. Liew and Q. Xiong, *Nat. Mater.*, 2021, **20**, 1315–1324.
4 T. Byrnes, N. Y. Kim and Y. Yamamoto, *Nat. Phys.*, 2014, **10**, 803–813.
5 H. Dong, C. Zhang, X. Liu, J. Yao and Y. S. Zhao, *Chem. Soc. Rev.*, 2020, **49**, 951–982.
6 R. Su, C. Diederichs, J. Wang, T. C. H. Liew, J. Zhao, S. Liu, W. Xu, Z. Chen and Q. Xiong, *Nano Lett.*, 2017, **17**, 3982–3988.
7 Q. Han, J. Wang, J. Lu, L. Sun, F. Lyu, H. Wang, Z. Chen and Z. Wang, *ACS Photonics*, 2020, **7**, 454–462.
8 M. A. Masharin, A. K. Samusev, A. A. Bogdanov, I. V. Iorsh, H. V. Demir and S. V. Makarov, *Adv. Funct. Mater.*, 2023, **33**, 2215007.
9 T. J. S. Evans, A. Schlaus, Y. Fu, X. Zhong, T. L. Atallah, M. S. Spencer, L. E. Brus, S. Jin and X. Y. Zhu, *Adv. Opt. Mater.*, 2018, **6**, 1700982.
10 Q. Shang, M. Li, L. Zhao, D. Chen, S. Zhang, S. Chen, P. Gao, C. Shen, J. Xing, G. Xing, B. Shen, X. Liu and Q. Zhang, *Nano Lett.*, 2020, **20**, 6636–6643.
11 J. Song, Q. Shang, X. Deng, Y. Liang, C. Li, X. Liu, Q. Xiong and Q. Zhang, *Adv. Mater.*, 2023, **35**, 2302170.
12 L. Protesescu, S. Yakunin, M. I. Bodnarchuk, F. Krieg, R. Caputo, C. H. Hendon, R. X. Yang, A. Walsh and M. V. Kovalenko, *Nano Lett.*, 2015, **15**, 3692–3696.
13 S. Yakunin, L. Protesescu, F. Krieg, M. I. Bodnarchuk, G. Nedelcu, M. Humer, G. D. Luca, M. Fiebig, W. Heiss and M. V. Kovalenko, *Nat. Commun.*, 2015, **6**, 8056.
14 J. Chen, W. Du, J. Shi, M. Li, Y. Wang, Q. Zhang and X. Liu, *InfoMat*, 2020, **2**, 170–183.
15 S. Zhang, Y. Zhong, F. Yang, Q. Cao, W. Du, J. Shi and X. Liu, *Photonics Res.*, 2020, **8**, A72–A90.
16 C. Bujalance, L. Calio, D. N. Dirin, D. O. Tiede, J. F. G. López, J. Feist, F. J. G. Vidal, M. V. Kovalenko and H. Míguez, *ACS Nano*, 2024, **18**, 4922.
17 D. Mao, L. Chen, Z. Sun, M. Zhang, Z. Y. Shi, Y. Hu, L. Zhang, J. Wu, H. Dong, W. Xie and H. Xu, *Light: Sci. Appl.*, 2024, **13**, 34.
18 L. K. Van Vugt, B. Piccione, C. H. Cho, P. Nukala and R. Agarwal, *Proc. Natl. Acad. Sci. U. S. A.*, 2011, **108**, 10050–10055.
19 M. C. Yen, C. Jg Lee, Y. C. Yao, Y. L. Chen, S. C. Wu, H. C. Hsu, Y. Kajino, G. R. Lin, K. Tamada and Y. J. Lee, *Adv. Opt. Mater.*, 2023, **11**, 2202326.
20 F. Krieg, P. C. Sercel, M. Burian, H. Andrusiv, M. I. Bodnarchuk, T. Stoferle, R. F. Mahrt, D. Naumenko, H. Amenitsch, G. Raino and M. V. Kovalenko, *ACS Cent. Sci.*, 2020, **7**, 135–144.
21 D. Baranov, A. Fieramosca, R. X. Yang, L. Polimeno, G. Lerario, S. Toso, C. Giansante, M. D. Giorgi, L. Z. Tan, D. Sanvitto and L. Manna, *ACS Nano*, 2020, **15**, 650–664.
22 J. Liu, X. Zheng, O. F. Mohammed and O. M. Bakr, *Acc. Chem. Res.*, 2022, **55**, 262–274.
23 L. Chen, B. Zhou, Y. Hu, H. Dong, G. Zhang, Y. Shi and L. Zhang, *Adv. Opt. Mater.*, 2022, **10**, 2200494.
24 L. Chen, D. Mao, Y. Hu, H. Dong, Y. Zhong, W. Xie, N. Mou, X. Li and L. Zhang, *Adv. Sci.*, 2023, **10**, 2301589.
25 T. V. Sekh, I. Cherniukh, E. Kobiyama, T. J. Sheehan, A. Manoli, C. Zhu, M. Athanasiou, M. Sergides, O. Ortikova, M. D. Rossell, F. Bertolotti, A. Guagliardi, N. Masciocchi, R. Erni, A. Othonos, G. Itskos, W. A. Tisdale, T. Stöferle, G. Raino, M. I. Bodnarchuk and M. V. Kovalenko, *ACS Nano*, 2024, **18**, 8423.
26 G. Rainò, M. A. Becker, M. I. Bodnarchuk, R. F. Mahrt, M. V. Kovalenko and T. Stöferle, *Nature*, 2018, **563**, 671–675.

27 C. Zhou, Y. Zhong, H. Dong, W. Zheng, J. Tan, Q. Jie, A. Pan, L. Zhang and W. Xie, *Nat. Commun.*, 2020, **11**, 329.
28 W. Du, S. Zhang, Q. Zhang and X. Liu, *Adv. Mater.*, 2019, **31**, 1804894.
29 Z. Lin, R. Huang, S. Li, S. Liu, J. Song, M. Panmai and S. Lan, *J. Phys. Chem. Lett.*, 2022, **13**, 9967.
30 M. Zhang, Z. Zheng, Q. Fu, Z. Chen, J. He, S. Zhang, L. Yan, Y. Hu and W. Luo, *CrystEngComm*, 2017, **19**, 6797–6803.
31 L. Chen, Y. Hu, B. Zhou, H. Dong, N. Mou, J. He, Z. Yang, J. Li, Z. Zhu and L. Zhang, *Adv. Mater. Interfaces*, 2022, **9**, 2200187.
32 D. Zhang, S. W. Eaton, Y. Yu, L. Dou and P. Yang, *J. Am. Chem. Soc.*, 2015, **137**, 9230–9233.
33 M. Liu, J. Zhao, Z. Luo, Z. Sun, N. Pan, H. Ding and X. Wang, *Chem. Mater.*, 2018, **30**, 5846–5852.
34 Y. E. Mendili, F. Grasset, N. Randrianantoandro, N. Nerambourg, J. M. Greneche and J. F. Bardeau, *J. Phys. Chem. C*, 2015, **119**, 10662–10668.
35 D. Baranov, M. J. Lynch, A. C. Curtis, A. R. Carollo, C. R. Douglass, A. M. M. Tejada and D. M. Jonas, *Chem. Mater.*, 2019, **31**, 1223–1230.
36 J. Qiu, H. Y. Hou, N. T. Huyen, I. S. Yang and X. B. Chen, *Appl. Sci.*, 2019, **9**, 2807.
37 C. Zhou, J. M. Pina, T. Zhu, D. H. Parmar, H. Chang, J. Yu, F. Yuan, G. Bappi, Y. Hou, X. Zheng, J. Abed, H. Chen, J. Zhang, Y. Gao, B. Chen, Y.-K. Wang, H. Chen, T. Zhang, S. Hoogland, M. I. Saidaminov, L. Sun, O. M. Bakr, H. Dong, L. Zhang and E. H. Sargent, *Adv. Sci.*, 2021, **8**, 2101125.
38 D. Rossi, H. Wang, Y. Dong, T. Qiao, X. Qian and D. H. Son, *ACS Nano*, 2018, **12**, 12436–12443.
39 B. R. C. Vale, E. Socie, A. B. Caminal, J. Bettini, M. A. Schiavon and J. E. Moser, *J. Phys. Chem. Lett.*, 2019, **11**, 387–394.
40 Q. Li, Y. Yang, W. Que and T. Lian, *Nano Lett.*, 2019, **19**, 5620–5627.
41 Z. Y. Wu, J. H. Zhuang, Y. T. Lin, Y. H. Chou, P. C. Wu, C. L. Wu, P. Chen and H. C. Hsu, *ACS Nano*, 2021, **15**, 19613–19620.
42 X. Li, Y. Wu, S. Zhang, B. Cai, Y. Gu, J. Song and H. Zeng, *Adv. Funct. Mater.*, 2016, **26**, 2435–2445.
43 Z. Liu, Q. Shang, C. Li, L. Zhao, Y. Gao, Q. Li, J. Chen, S. Zhang, X. Liu, Y. Fu and Q. Zhang, *Appl. Phys. Lett.*, 2019, **114**, 101902.
44 S. Wang, J. Ma, W. Li, J. Wang, H. Wang, H. Shen, J. Li, J. Wang, H. Luo and D. Li, *J. Phys. Chem. Lett.*, 2019, **10**, 2546–2553.
45 E. Y. Tiguntseva, D. G. Baranov, A. P. Pushkarev, B. Munkhbat, F. Komissarenko, M. Franckevicius, A. A. Zakhidov, T. Shegai, Y. S. Kivshar and S. V. Makarov, *Nano Lett.*, 2018, **18**, 5522–5529.
46 H. Li, Y. Xu, J. Xiang, X. F. Li, C. Y. Zhang, S. L. Tie and S. Lan, *Nanoscale*, 2016, **8**, 18963–18971.
47 S. Kushida, D. Okada, F. Sasaki, Z. H. Lin, J. S. Huang and Y. Yamamoto, *Adv. Opt. Mater.*, 2017, **5**, 1700123.
48 S. Li, M. Yuan, W. Zhuang, X. Zhao, S. Tie, J. Xiang and S. Lan, *Laser Photonics Rev.*, 2021, **15**, 2000480.
49 K. Park, J. W. Lee, J. D. Kim, N. S. Han, D. M. Jang, S. Jeong, J. Park and J. K. Song, *J. Phys. Chem. Lett.*, 2016, **7**, 3703.
50 S. Makarov, A. Furasova, E. Tiguntseva, A. Hemmetter, A. Berestennikov, A. Pushkarev, A. Zakhidov and Y. Kivshar, *Adv. Opt. Mater.*, 2019, **7**, 1800784.
51 Q. Zhang, R. Su, X. Liu, J. Xing, T. C. Sum and Q. Xiong, *Adv. Funct. Mater.*, 2016, **26**, 6238–6245.
52 Q. Li, C. Li, Q. Shang, L. Zhao, S. Zhang, Y. Gao, X. Liu, X. Wang and Q. Zhang, *J. Chem. Phys.*, 2019, **151**, 211101.